Electrochemistry Communications 138 (2022) 107280

Contents lists available at ScienceDirect

Electrochemistry Communications

journal homepage: www.elsevier.com/locate/elecom

Self-organized TiO_2 nanotubes on Ti-Nb-Fe alloys for biomedical applications: Synthesis and characterization

Juliana Rios [a], Victor N. Santini [a], Karina D. Pereira [a], Augusto D. Luchessi [a,c], Éder S.N. Lopes [b], Rubens Caram [b], Alessandra Cremasco [a,*]

[a] University of Campinas (UNICAMP), School of Applied Sciences, Limeira, SP 13484350, Brazil
[b] University of Campinas (UNICAMP), School of Mechanical Engineering, Campinas, SP 13083-860, Brazil
[c] São Paulo State University (UNESP), Institute of Biosciences, Rio Claro, SP 13506-900, Brazil

ARTICLE INFO

Keywords:
TiO_2 nanotubes
Anodization
Crystallization
Doping
Cell-material interaction

ABSTRACT

Titanium-based biomaterials with a self-organized titanium oxide (TiO_2) surface have received considerable attention in recent years owing to enhanced cellular response and bactericidal behavior promoted by the nanostructured surface. The aim of this study was to investigate the effect of Fe addition on the formation and crystallization of TiO_2 nanotubes on Ti-30Nb-xFe substrates and the effect of TiO_2 crystallinity on biological behavior. Self-ordered TiO_2 nanotubes were prepared by anodization of Ti-30Nb-xFe (x = 0, 3, and 5 wt%) alloys using an aqueous 0.3% HF (vol.%) electrolyte. The nanotube morphology, structure, and composition as a function of the annealing temperature were characterized using FE-SEM, XRD and XPS. The crystallization of nanotubes to the rutile phase occurred at similar temperatures for samples with or without Fe addition, and a mixture of anatase and rutile was observed at 675 °C. The cell viability profile on different surfaces was investigated by MTT and adhesion assays, which revealed improved *in vitro* response to the crystalline nanotubes.

1. Introduction

Titanium and its alloys are commonly used as implant materials owing to their excellent properties, such as a high strength-to-weight ratio, low elastic modulus, and superior corrosion resistance to physiological fluids [1]. Some β-Ti-type alloys have exhibited promise as biomaterials for load-bearing implants, among which, Ti-Nb alloys have attracted considerable attention in recent years. Nb is a highly biocompatible, β-stabilizing element, and its addition to Ti allows the retention of the β phase at room temperature, producing a material with a very low elastic modulus, which minimizes stress shielding and bone reabsorption [2–4]. The results of a recent study on Fe-added Ti-Nb alloys indicated that they are promising candidates for biomedical applications. Literature suggests that Ti-Nb-Fe alloys impart mechanical strength combined with a low elastic modulus.

Chaves et al. (2015) explored Ti-xNb-3Fe (x = 10, 15, 20, and 25 wt %) alloys that were melted and then rapidly solidified; among these, the Ti-25Nb-3Fe alloy exhibited the lowest elastic modulus of approximately 65 GPa [5]. Ehtemam–Haghighi et al. (2016) reported the results for Ti-11Nb-xFe (x = 0.5, 3.5, 6, and 9 wt%) alloys that were melted via cold crucible levitation melting (CCLM). They found that the compressive yield strength and Vickers hardness ranged from 796 to 1137 MPa and 278 to 357 HV, respectively. The full β-Ti-11Nb-9Fe alloy exhibited the lowest elastic modulus (82 GPa) and highest elongation at fracture (38%). The results indicated that the elastic modulus of the alloys decreased with the addition of Fe, which is a powerful β-stabilizing element. Meanwhile, the plastic strain and elastic energy were enhanced owing to the retained β phase [6]. Lopes et al. (2016) investigated Ti-30Nb-xFe (x = 0, 1, 3, 5 wt%) alloys, which have a higher Nb content, and obtained an elastic modulus as low as 80 GPa. The addition of 5 wt% Fe improves the ultimate final tensile strength from 601 to 689 MPa but reduces the elongation at fracture from 28% to 16%. They also found that Fe additions above 3% increased corrosion resistance [7]. Biesiekierski et al. (2016) melted a Ti-12Nb-5Fe alloy via CCLM and reported an elastic modulus, compressive strength, and elongation at fracture of 90 GPa, >1000 MPa, and >40%, respectively, which agree well with those of commercial implantable metals [9]. In addition, the electrochemical and cell proliferation behaviors were satisfactory for biomedical applications [8]. Li et al. (2019) investigated Ti-(14, 16, 18, 20, 22, and 24)Nb-2Fe (at.%) alloys and revealed the coexistence of the ω and α″

* Corresponding author.
E-mail address: acremasc@unicamp.br (A. Cremasco).

https://doi.org/10.1016/j.elecom.2022.107280

Available online 18 April 2022

phases in the β-quenched Ti-14Nb-2Fe alloy, while other compositions only presented a single β phase. The results indicated a considerable solid-solution strengthening effect in the studied alloys [10].

However, despite their interesting mechanical properties, these materials exhibit poor interactions with the surrounding tissues, which may eventually result in implant failure [11,12]. The surface characteristics of metallic implants strongly influence the tissue–implant biological interactions [13]. The formation of a porous nanostructured oxide layer on Ti-based implants is an effective surface modification strategy to improve their biofunctional properties. The growth of the bone tissue surrounding the implant depends on the interfacial morphology and micro- and nanoscale chemical aspects [12,14], including other surface features, such as hydrophilicity, which plays an important role in bone response [15]. In addition, the crystalline features of the oxide layer on Ti-based implants affect the rates of proliferation and differentiation of cells [14]. Studies have shown that a mixture of anatase and rutile phases exhibits better biocompatibility than that exhibited by amorphous NTs [16,17]; furthermore, they have indicated the superior behavior of a fully anatase structure [18–20]. Therefore, there is no consensus on how crystalline structures affect cell activity and which phase or phase combination is most effective (anatase or a mixture of anatase/rutile) for improving cell activity. It is worth noting that most studies in the literature have been conducted with NTs grown on pure Ti, which present different surface chemistry, topography, and wettability.

Anodization is one of the most viable and environmentally friendly methods for producing oxide NT arrays with tunable dimensions and morphologies [21]. Several theories, such as field-assisted dissolution (FAD) theory and its variations [22,23], have been proposed to explain the formation and growth of NTs. The FAD model is based on competing oxidation and dissolution processes [24]. Recently, the oxygen bubble model has been revisited and applied to better explain NT formation in three stages: (i) barrier oxide layer formation, (ii) pore initiation, and (iii) self-organized NT growth. Although the FAD model indicates that these three stages are influenced by the anodizing conditions, such as the applied voltage, electrolyte type, temperature, and anodization time [21,25–27] it does not properly explain the morphology and current evolution of the steady state associated with the dissolution reaction, resulting in only a qualitative elucidation. According to the oxygen bubble model, the ionic current promotes oxide growth, while the electronic current produced by oxygen evolution maintains the NT growth. The expansion of oxygen bubbles entrapped between the oxide compact layer and electrolyte–oxide interface as well as the volume expansion of stress oxide lead to a deformation of the compact oxide layer, forming a hemispherical bottom that acts as a mold for the NTs. When the oxygen release and oxide growth rates reach equilibrium, stage III occurs [22,23].

Additional factors that control the growth of the nanostructured oxide layer are the chemical composition and microstructure of the substrate [28,29]. Inhomogeneous dissolution caused by a highly acidic electrolyte is typically observed in a dual-phase microstructure because of the heterogeneous alloying element distribution [30]. In Ti alloys with an α + β or α'+β microstructure, a nanoporous oxide is often formed in the Ti-poor β phase region, while a nanotubular morphology is observed in the Ti-rich α or α" phase region [28,29]. The grain size and texture of the substrate can also affect the TiO_2 NT morphology. Hu et al. (2016) evaluated TiO_2 NTs formed on pure Ti processed by high-pressure torsion and observed that a decrease in grain size resulted in an increase in NT layer thickness and a more homogeneous NT size distribution [31]. An increase in the number of crystalline defects, such as vacancies and dislocations, causes a change in the free energy, which favors nucleation and oxide layer growth.

Some physical properties, such as the free surface of nanostructured oxides, are known to depend on defects, such as grain boundaries and doping atoms in the oxide layer. Several studies related to TiO_2 NT formation and its properties have been conducted using pure Ti, commercial alloys, such as Ti-6Al-4V [32] and Ti-6Al-7Nb [28,33,34], as well as other experimental alloys based on Ti-Nb [35] and Ti-Zr systems [36]. However, studies regarding TiO_2 NT formation on Ti-Nb-Fe alloys are lacking, and the addition of Fe to Ti-Nb alloys may change the electrochemical properties, including the anodization process.

Therefore, in this study, the effects of Fe addition on the formation and crystallization of TiO_2 NTs on Ti-30Nb-xFe substrates were investigated. In addition, the influence of TiO_2 crystallinity on the cell viability profile was discussed based on MTT and cellular adhesion assays.

Table 1
Chemical composition measure by XRF (wt.%).

Nominal composition	Measured composition		
	Ti	Nb	Fe
Ti-30Nb	Bal.	29.5 ± 0.2	0.06 ± 0.01
Ti-30Nb-3Fe	Bal.	29.1 ± 0.6	2.8 ± 0.6
Ti-30Nb-5Fe	Bal.	29.1 ± 0.2	5.5 ± 0.3

2. Material and methods

Ti-30Nb-xFe (x = 0, 3, 5 wt%) ingots were prepared by arc melting from of high-purity (99.99%) Ti, Nb, and Fe, using non-consumable tungsten electrode under argon atmosphere, homogenized at 1000 °C for 12 h, followed by furnace cooling. These ingots were subjected to plastic deformation by hot rolling and sectioned using a precision machine (Accutom-10, Struers, Dennmark) to obtain samples with dimensions of 10 mm × 10 mm × 2.5 mm. The samples were sealed in a quartz tube under high-purity argon atmosphere and subjected to solution heat treatment at 1000 °C for 1 h and water-quenched (ST/WQ).

The chemical composition of the alloys, measured using energy dispersive X-ray fluorescence spectroscopy (XRF) (EDX-7000, Shimadzu, Japan), is shown in Table 1. The interstitial elements O and N are within Ti Grade 2 limits (O ≤ 0.25, N ≤ 0.03), and these results, including substrate microstructure characterization, have been reported in a previous work [7].

Self-organized TiO_2 was produced by anodization using a potentiostat (Autolab PGSTAT302N, Metrohm, Netherlands), and a two-electrode cell with a Pt sheet and Ti-Nb-Fe-based samples as the cathode and anode, respectively. The experiments were conducted using a 0.3% HF (vol.%) electrolyte solution under stirring at room temperature by applying a voltage of 20 V for 60 min. Prior to anodization, the samples were polished using SiC grit paper (#400 and #1200), degreased by sonication in isopropyl alcohol and deionized water for 10 min, and dried in a nitrogen flux. The morphology and dimensions of NTs were analyzed using field emission scanning electron microscopy (FE-SEM) (Magellan 400 L, FEI, USA) and ImageJ® software, respectively.

For TiO_2 NT phase transformations, the samples were subjected to isothermal annealing (500–675 °C, 10 °C/min, air atmosphere) for 1 h in a homemade resistive furnace. The TiO_2 polymorphism was analyzed using the grazing-incidence X-ray diffraction (XRD) technique (X'Pert PRO, PANalytical, Netherlands) with Cu-Kα radiation (30 kV, 40 mA, λ = 0.15418 nm, grazing angle = 2°, 20° < 2θ < 60°).

Anodized and heat-treated Ti-30Nb-3Fe substrates were selected to investigate their morphology, chemical composition, wettability, and biological behavior for application as biomaterials. Therefore, the samples were heated at temperatures in which the TiO_2 polymorphic arrangement was composed of 100% anatase or a mixture of nearly 50% anatase and 50% rutile. Characterization of the TiO_2 NT surface after crystallization annealing was performed using FE-SEM. The chemical composition and relative fraction of oxides were determined using X-ray photoelectron spectroscopy (XPS) (K-Alpha, Thermo Fisher Scientific Inc., USA). The sample surface was sputtered with an Ar^+ ion beam for

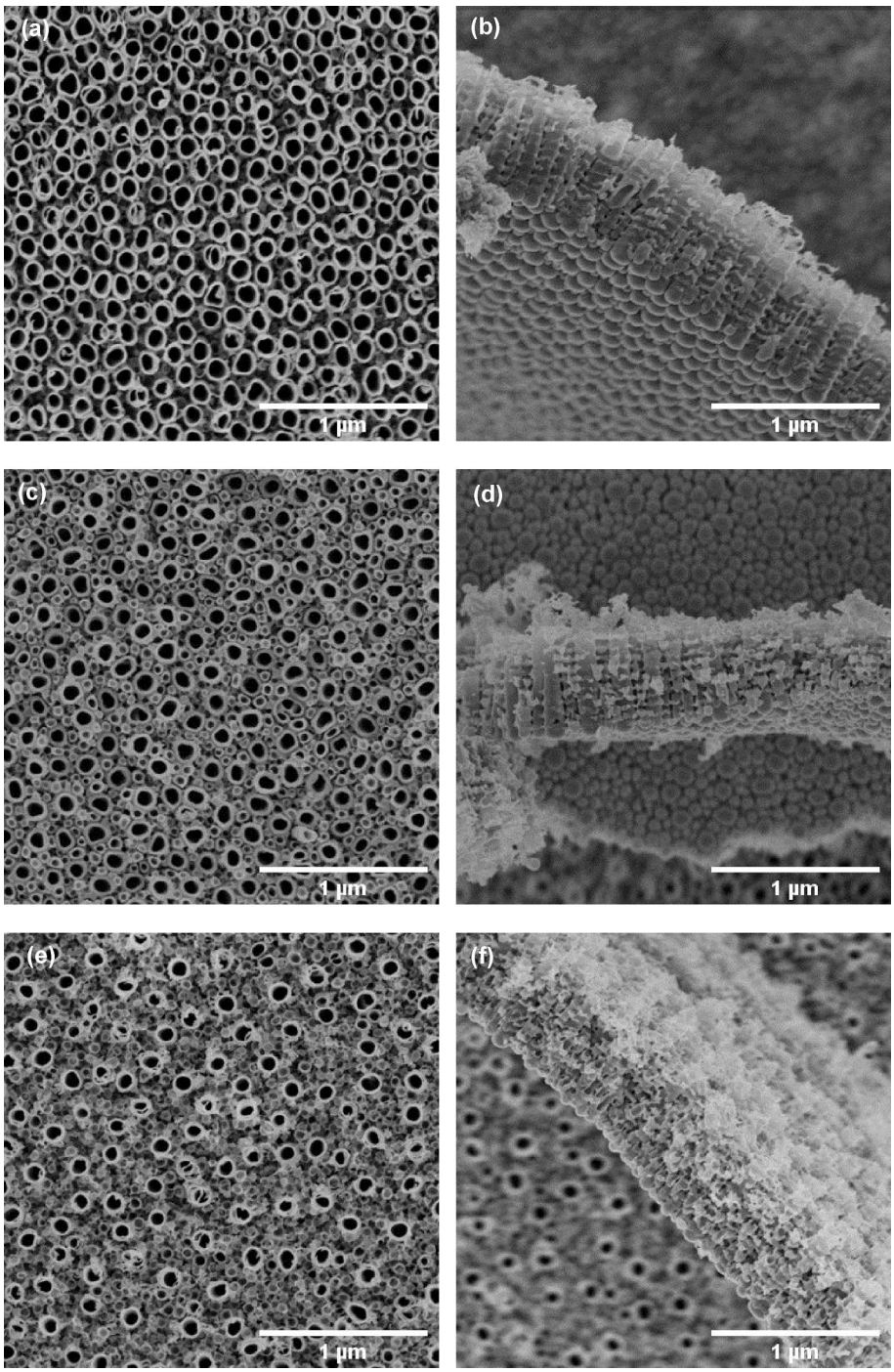

Fig. 1. FE-SEM micrography of TiO_2 nanotubes formed by electrochemical anodization on (a-b) Ti-30Nb (c-d) Ti-30Nb-3Fe (e-f) Ti-30Nb-5Fe ST/WQ samples.

60 s to remove any surface contamination prior to XPS analysis.

The water contact angle (WCA) was investigated to evaluate the wetting properties of the samples. Measurements were performed at room temperature in static mode using a sessile drop method in an optical tensiometer (OCA, DataPhysics Instruments, Germany) using distilled water as the fluid. The average value was calculated from at least three measurements for each sample.

The myoblast cell line C2C12, a pre-osteoblastic cell line that can be differentiated by bone morphogenic protein 2 (BMP-2), was cultured in DMEM medium containing 10% fetal bovine serum (FBS), supplemented with 2 mM L-glutamine, 100 U/ml penicillin, and 100 µg/ml streptomycin (Life Technologies, Inc., Carlsbad, CA, USA) in a humidified incubator at 37 °C with 5% CO_2. Cell subcultures were performed every two days until the beginning of the experiment. C2C12 cells with 80% confluency were trypsinized and then inactivated with DMEM containing FBS. Discs containing nanomaterials previously autoclaved at 121 °C for 15 min were placed in 24 well plates (1 disc per well). Next, 60 µL of cellular suspension (1×10^5 cells) were dripped on each disc, with a sufficient volume to cover the discs. The plates were incubated in a humidified incubator at 37 °C with 5% CO_2 for 2 h to enable cell adhesion to discs. Then, 1 ml of DMEM containing FBS was added to each well and the plates were returned to incubator.

The cell viability profile was assessed by 3-(4,5-dimethylthiazol-2-yl)-2,5-diphenyltetrazolium bromide (MTT) assay. After 48 h of plating, the discs were transferred to fresh 24 well plates, and then 200 µL of MTT solution (0.5 mg/mL) diluted with 1X phosphate-buffered saline

Table 2
General dimensions of TiO_2 nanotubes fabricated through electrochemical anodization on Ti-30Nb, Ti-30Nb-3Fe andTi-30Nb-5Fe ST/WQ substrates.

Substrates	Conditions of NTs	Tube dimensions (nm)		
		Inner diameter	Outer diameter	Tube length
Ti-30Nb	as-prepared	89 ± 9	133 ± 7	735 ± 39
Ti-30Nb-3Fe	as-prepared	87 ± 10 / 39 ± 6	131 ± 13 / 79 ± 9	576 ± 47
Ti-30Nb-5Fe	as-prepared	76 ± 9 / 44 ± 5	120 ± 10 / 71 ± 6	490 ± 50

(PBS) was added to the wells, followed by incubation at 37 °C for 2 h. The MTT solution was removed and 400 μL of dimethyl sulfoxide (DMSO) was added to each well of the treated cells to dissolve the formazan crystals. The absorbance at 570 nm was measured using a spectrophotometer (Epoch Microplate Spectrophotometer, BioTek Instruments, USA). All the chemical reagents used were acquired from Life Technologies, USA.

The cellular morphology was analyzed after 24 h of culture. The cells on the substrate were washed with PBS and fixed in a 2.5% glutaraldehyde solution for 2 h. Afterward, the cells were washed with PBS solution for 15 min, three times each. Then, the cells were dehydrated in

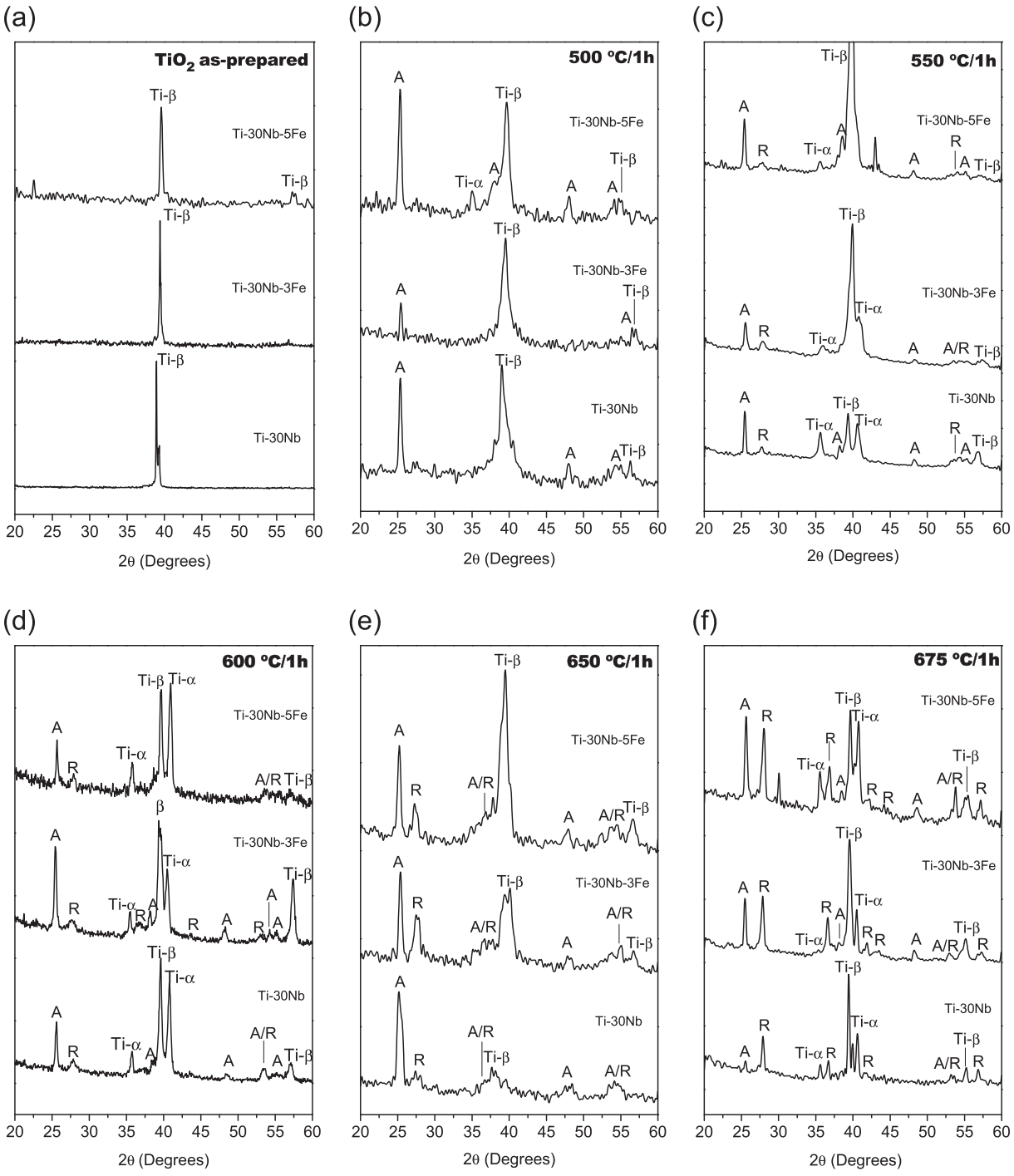

Fig. 2. Glazing-angle XRD patterns of TiO_2 nanotube layers formed on Ti-30Nb-xFe substrates as-fabricated and after heat treatments in temperatures between 500 °C and 675 °C for 1 h.

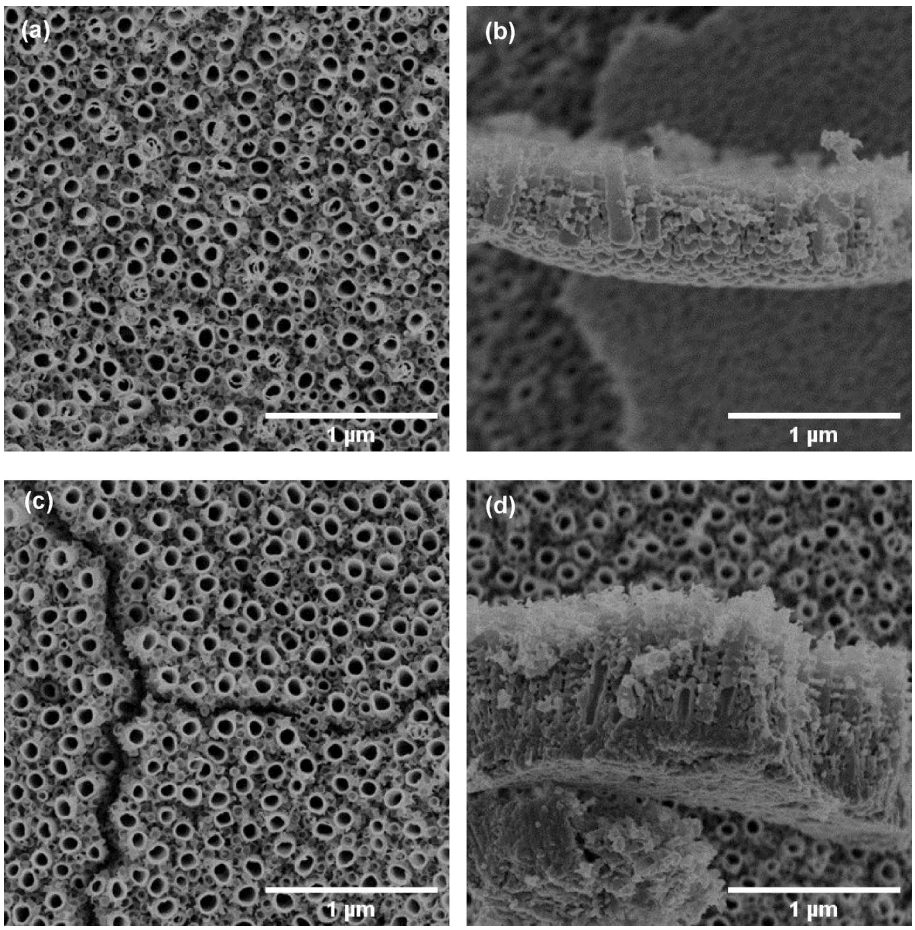

Fig. 3. FE-SEM micrographs of TiO_2 nanotubes formed by electrochemical anodization in 0.3%HF electrolyte on Ti-30Nb-3Fe substrates and then, heat treated at 500 °C (a-b) and 675 °C (c-d) for 1 h.

a sequence of aqueous ethanol solutions (50, 70, 95, and 100% v/v) for 15 min each and dried at the critical point. The dried cells were subjected to sputter-coated with gold for the FE-SEM analysis.

3. Results and discussion

The SEM and XRD analyses of the Ti-30Nb-xFe samples revealed an α" martensite phase mixed with β phase matrix in Ti-30Nb alloy and a fully β phase in alloys containing 3 and 5 wt% Fe. However, in a previous study, a detailed analysis by TEM indicated the ω_{ath} phase in all the studied alloys [7].

The morphology of self-organized TiO_2 layers, produced by anodization, are shown on their surface and cross-sectional FE-SEM images (Fig. 1). A nanotubular structure was formed on all substrates. The NTs obtained on the Ti-30Nb substrate had an inner and outer diameter of 90 and 130 nm, respectively, and a length of approximately 700 nm. A bimodal NT size distribution was observed on substrates containing Fe, where the larger NTs were surrounded by smaller ones. However, a decrease in the NT length (to approximately 500 nm) and a slight decrease in diameter were observed in the samples with Fe content. The bimodal feature is related to (i) iron oxide combined with other oxides (TiO_2 and Nb_2O_5) of different dissolution rate and (ii.) Nb and Fe doping of TiO_2 nanotubes. Table 2 summarizes the quantitative measurements of the NT dimensions. The bimodal feature was also observed in Ti-(50–80)Zr [37] and Ti-(20–40)Nb [35] alloys and was more pronounced in samples with higher amounts of alloying elements.

Alternatively, an uneven field distribution model proposed by Ozkan et al. could also explain the arrangement in a two-size scale, as observed in this work [38,39]. Other possible reasons are the mold effect of oxygen bubbles and the plastic flow of oxide doped with Nb/Fe, which directly affect the formation of NT embryos [22,23]. However, the exact mechanism underlying this phenomenon requires further clarification.

The TiO_2 NT layer showed an amorphous structure, as revealed by the corresponding XRD patterns (Fig. 2(a)). To mitigate the low mechanical stability caused by the weak adhesion of the nanostructured layer to the substrate surface, further heat treatments are required [40]. Usually, samples are heated to a temperature above 400 °C to induce structural transition from the amorphous to crystalline phase without modifying the NT diameter [14], although some change in wall thickness is observed [13]. Additionally, this procedure could also increase the wettability and, hence, improve the biological surface properties of the substrate [13,14].

To promote TiO_2 NT layer crystallization, isothermal annealing was performed as described earlier. The annealing at 500 °C resulted in a fully anatase phase on all the surfaces investigated. At 550 °C, a small amount of rutile mixed with the predominant anatase phase was observed on all the samples, and its fraction increased as the temperature rose to 675 °C. At the highest temperature (675 °C), the samples containing Fe exhibited TiO_2 NTs with comparable anatase and rutile fractions, while the Ti-30Nb sample presented an almost fully rutile structure.

The effect of annealing on the TiO_2 NT morphology was also analyzed using FE-SEM (Fig. 3). The morphologies correspond to the NTs obtained on Ti-30Nb-3Fe substrates that were heated at 500 °C forming anatase (Fig. 3 (a-b)), and at 675 °C forming an anatase/rutile mixture (Fig. 3 (c-d)).

As observed, a uniform and crack-free layer of anatase with a bimodal distribution of NTs was maintained even after annealing. By

Table 3
Typical TiO_2 nanotube dimensions obtained by electrochemical anodization and heat treated at 500 and 675 °C for 1 h on Ti-30Nb-3Fe substrates.

Substrates	Conditions	Tube dimensions (nm)		
		Inner diameter	Outer diameter	Length
Ti-30Nb-3Fe	as-prepared	87 ± 10 / 39 ± 6	131 ± 13 / 79 ± 9	576 ± 47
	500 °C/1h	85 ± 10 / 52 ± 9	129 ± 10 / 79 ± 9	584 ± 57
	675 °C/1h	84 ± 11 / 40 ± 5	136 ± 14 / 81 ± 9	950 ± 92

contrast, the layer formed by the anatase/rutile mixture showed several cracks, which could be attributed to the volumetric difference between the two phases [41]. Another possible origin of cracks is related to an increase in the internal stress induced by the structural transformation [42]. It was also found that a higher annealing temperature resulted in an increase in the interfacial region between the TiO_2 NTs and the substrate. According to Roguska et al. (2016), this probably occurs due to further substrate oxidation coupled with sintering between the NT layers and the substrate during the high-temperature treatment [14]. In addition to the phase transition, annealing also modifies the porosity, which changes the surface characteristics of the nanostructured layer [43].

When comparing dimensional parameters such as inner and outer NT diameters before and after annealing, no significant differences were observed (Table 3). However, NTs composed of anatase/rutile mixture, which were heated at 675 °C, exhibited a significant increase in length, probably due to additional oxidation during the high-temperature exposure. As the annealing temperature increased, another TiO_2 layer formed between the nanostructured layer and the substrate. This

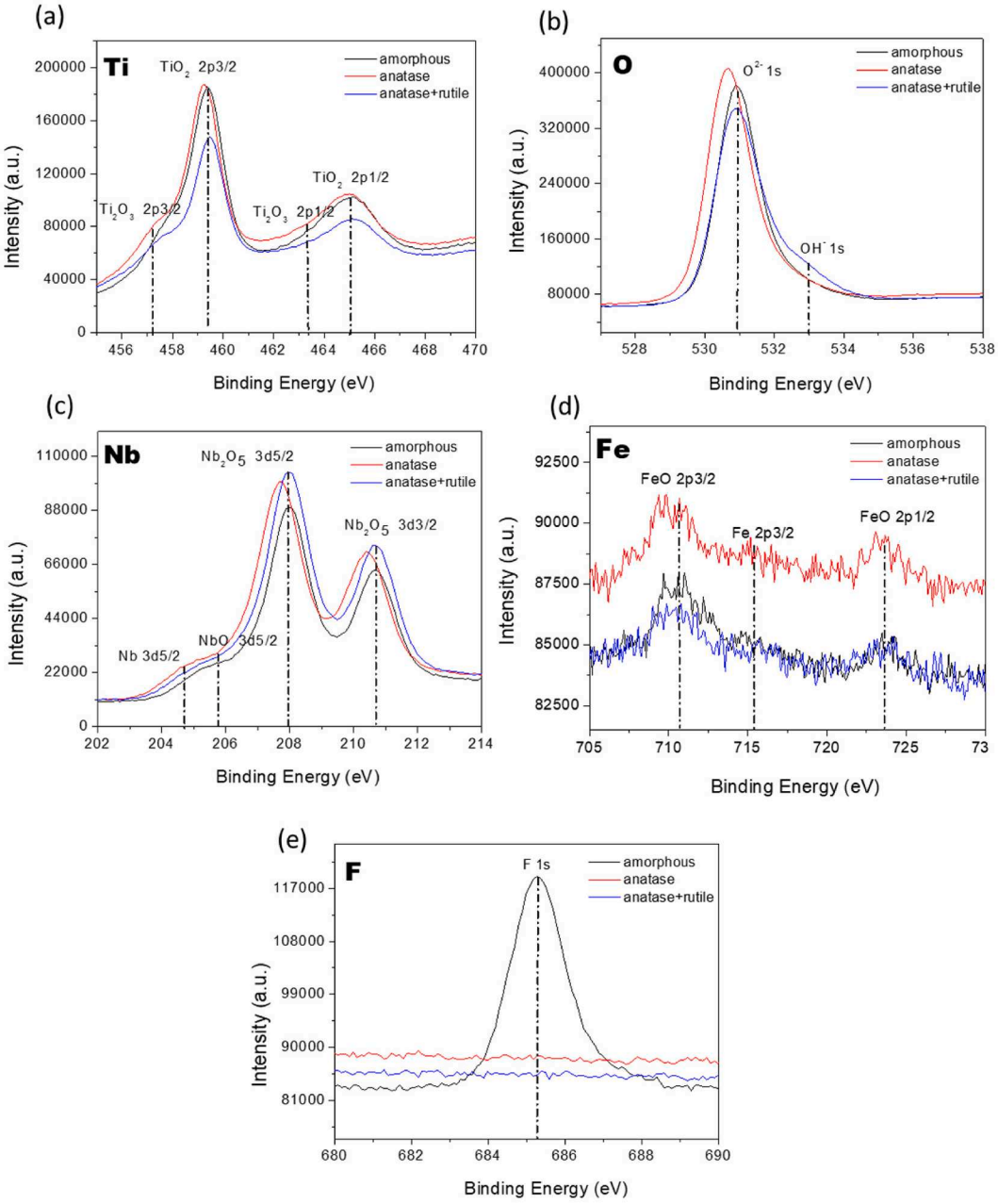

Fig. 4. XPS spectra obtained on anodized Ti-30Nb-3Fe samples coated with TiO_2 NTs: (a) Ti 2p, (b) O 1 s, (c) Nb 3d, (d) Fe 2p and (e) F 1 s. Black line: as-fabricated; red line: annealed at 500 °C; blue line: annealed at 675 °C. (For interpretation of the references to colour in this figure legend, the reader is referred to the web version of this article.)

Table 4
Relative elemental composition of the nanotube oxide layer determined by XPS.

Conditions		Element (at. %)					
		Ti	O	Ti/O	Nb	Fe	F
as-prepared	Amorphous	19.6	63.8	0.307	9.9	0.5	6.2
500 °C/1h	Anatase	19.6	68.0	0.288	11.3	1.1	–
675 °C/1h	Anatase/rutile	15.8	70.9	0.223	12.8	0.5	–

additional layer is mainly composed of the rutile phase, and its thickness increases with the temperature [44]. The nanotubular structure was still observed after this additional oxidation, evidently with no collapse or coalescence, although a few cracks were observed, as previously mentioned.

XPS measurements were carried out on Ti-30Nb-3Fe samples coated with TiO_2 NTs under three different surface conditions, i.e., amorphous (as-prepared), fully anatase (500 °C), and anatase/rutile mixture (675 °C). The XPS spectra (Fig. 4) indicate the binding energies of O 1s, Ti 2p, Nb 3d, and Fe 3d, corresponding to TiO_2, Nb_2O_5, and FeO oxides, respectively. The peak corresponding to F 1s (Fig. 4(e)) in the amorphous samples originates from the electrolyte incorporated into the NTs during anodization. After annealing at both temperatures (500 °C and 675 °C), it was completely eliminated as a volatile component [45], and therefore, the peak also disappeared. The results of XPS measurements conducted by Xu et al. (2012) on TiO_2 NTs formed on CP-Ti and Ti-20Nb (at.%) samples revealed a substitutional doping of high-valence transition-metal ions (Nb^{5+}) into TiO_2, which causes a positive shift of Ti 2p and O 1s peaks, as observed in this work [30].

The annealing process affected the fraction of oxides on the substrate surface, as a decrease in the TiO_2 fraction and an increase in Nb oxides was observed after annealing at 675 °C. A higher amount of FeO was observed in the samples annealed at 500 °C. This caused a slight shift toward lower binding energy due to Nb and Fe oxides, which indicates that Fe^{2+} is incorporated into the TiO_2 lattice, replacing Ti^{4+} ions and forming Fe–O–Ti bonds [46]. The relative amounts of oxides (Table 4) indicate that the cationic level in oxide films is lower than that in bulk samples. In addition, post annealing, the O 1s peak increased, while that corresponding to Ti 2p decreased. The annealing caused an increase in the oxygen content due to decrease in oxygen vacancies and oxidation of Ti^{3+} to Ti^{4+} [43].

The nanostructured surfaces on Ti-30Nb-3Fe substrates with different characteristics were investigated for use as biomaterials whose wettability is directly related to cell adhesion and protein adsorption [43]. The contact angle measurements (Fig. 5) indicated that polished non-anodized (WCA = 71°) are less hydrophilic than TiO_2 NTs samples. This phenomenon is expected due to an increase in surface area after anodization that promotes higher hydrophilicity [14,43], although an earlier study [47] on anodized Ti-6Al-4 V using organic-electrolyte resulted in hydrophobic surfaces.

It is known that in anodization using an ethylene glycol-based electrolyte, the formation of $Ti(OH)_4$ instead of TiO_2 can increase the hydrophobicity. In this case, natural aging can induce $Ti(OH)_4$ oxidation, producing TiO_2 according to the reaction:

$$Ti(OH)_4 \rightarrow TiO_2 + H_2O$$

Also, Shin et al. (2011) observed that TiO_2 nanotubes became more hydrophobic after a natural aging for three months. They found that the contact angle changes from 24 to 42 ° [48].

Annealing at a lower temperature (500 °C) significantly decreased the contact angle (WCA = 5°), suggesting superhydrophilicity due to anatase formation [37]. However, a higher annealing temperature (675 °C) led to the coexistence of anatase and rutile phases, inducing a negligible increase in contact angle (WCA = 10°). This slight change could be attributed to the rutile precipitation and crack formation in the nanostructured layer. The gradual loss of hydrophilicity when anatase/rutile phases coexist were observed by Chaves et al. (2016) which attributed to growth of rutile phase, that partially break the nanostructure [49]. These defects can take off locally the films from substrate and retain air at interface, it prevents that liquid permeates the surface. The residual fluoride present in the electrolyte also affects hydrophilicity [14,43,50].

The biocompatibility capacity was performed by combining the assessment of MTT assay, cellular adhesion, and morphology. The cell viability profile of samples covered with TiO_2 NTs (annealed at 500 °C

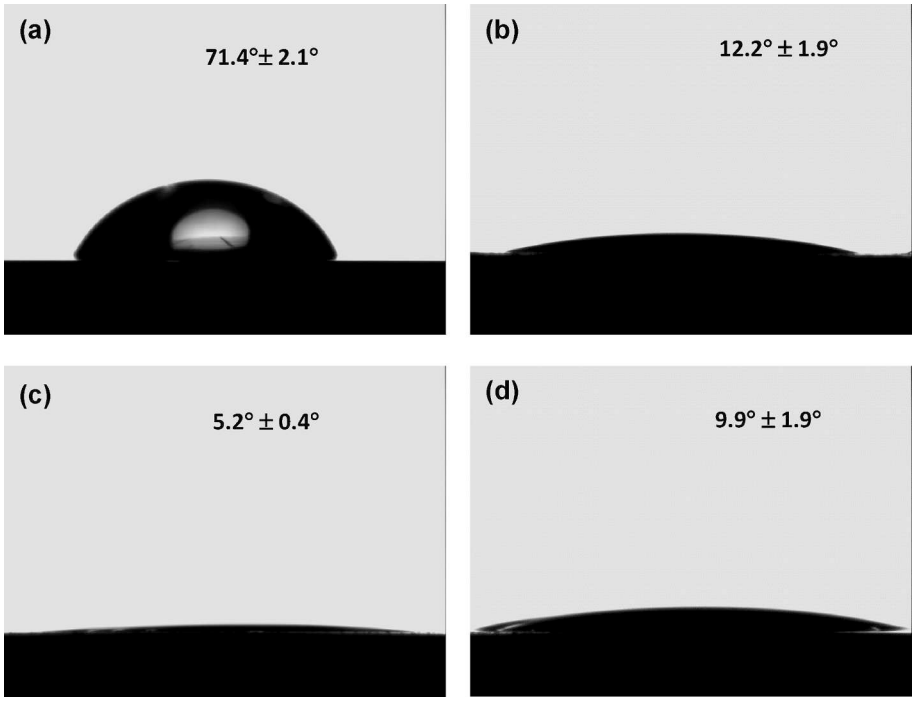

Fig. 5. Water contact angles for Ti-30Nb-3Fe substrate surface: (a) polished non-anodized; (b) amorphous TiO_2 NTs; (c) TiO_2 NTs annealed at 500 °C and (d) TiO_2 NTs annealed at 675 °C.

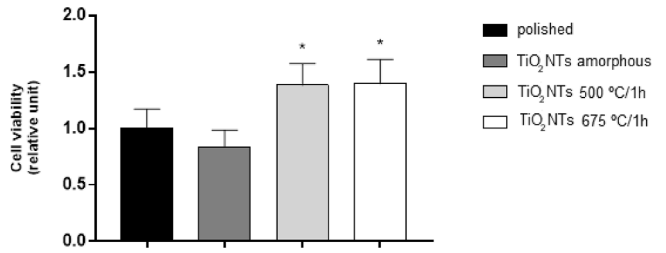

Fig. 6. Cell viability profile was performed using the 3-(4, 5-dimethylthiazol-2-yl)-2, 5-diphenyltetrazolium bromide (MTT) assay. The data shown are representative of four independent experiments. Statistically significant differences of the TiO_2 NTs annealed at 500 °C and TiO_2 NTs annealed at 675 °C compared with polished non-anodized are indicated by * ($p < 0.05$).

and 675 °C, showing TiO_2 crystalline forms) was approximately 1.5 times higher ($p < 0.05$) than that of polished non-anodized or amorphous NT surfaces (Fig. 6), as indirect measurement based on metabolic activity characterized by MTT assay. However, no difference in cell viability was observed between the TiO_2 NTs with anatase and anatase/rutile mixture.

Biological studies carried out with substrates showing TiO_2 NTs with different diameters (30–100 nm) revealed that a smaller diameter promotes the highest degree of cellular adhesion. A higher NT diameter increased the up-regulation of alkaline phosphatase activity, which is related to bone-forming ability [51].

The FE-SEM images of the C2C12 cells cultured on the surfaces of Ti-30Nb-3Fe substrates (Fig. 7) suggested a flat spread of cells. Cell profile on samples with polished non-anodized surfaces or covered with TiO_2 NTs under amorphous or crystalline conditions were very similar. The cells exhibited a rough dorsal surface, hard filopodia extension at the leading edge, and overlapping of adjacent cells, which indicates a healthy growth. The higher-magnification FE-SEM images revealed cellular extensions of numerous cells interacting with the NTs.

The increase in surface area of the Ti-Nb-Fe substrates with crystalline nanofeatures produced by anodization and annealing was found to be beneficial for cellular proliferation and adhesion. The reduced cell viability in amorphous TiO_2 NTs compared to crystalline ones is probably due to residual fluorine within the pores, introduced during the anodization process, it decomposes during the annealing process (Fig. 4 (e)) as also related to aspects topography and physical–chemical of the surface.

4. Conclusions

In summary, TiO_2 NTs were synthesized via anodization of Ti-30Nb samples containing Fe up to 5 wt% and using 0.3% HF electrolyte. The addition of Fe resulted in a nanostructured layer with a bimodal size distribution, which could be attributed to different oxide dissolution rates combined with uneven field distribution. Various oxide compositions were confirmed by XPS measurements, indicating NT doping with Nb_2O_5 and FeO. It was found that Fe addition stabilizes the anatase form after annealing at higher temperatures, maintaining nanotubular morphology up to 500 °C with superior hydrophilicity. The MTT assay and adhesion tests revealed that the TiO_2 NT layer formed by anatase or anatase/rutile mixture was more beneficial for cell viability, based on metabolic activity, and attachment when compared to Ti-30Nb-3Fe

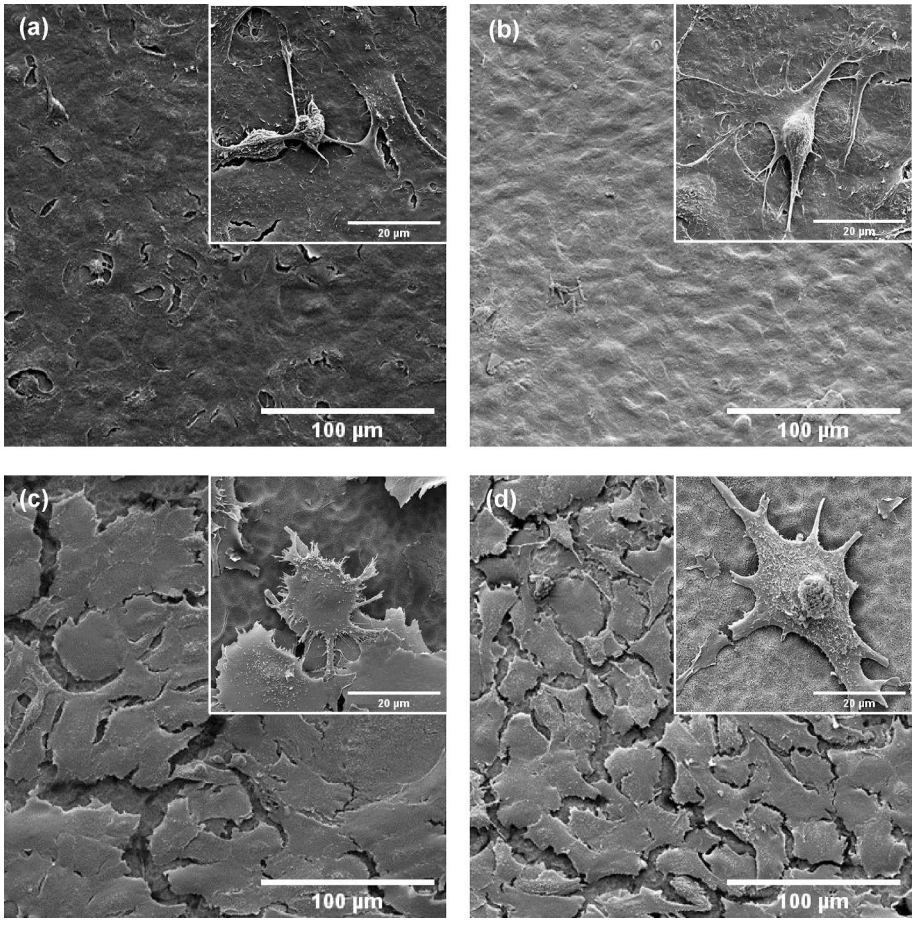

Fig. 7. FE-SEM image showing cell cultured on Ti-30Nb-3Fe substrate: (a) polished non-anodized; (b) TiO_2 NTs amorphous; (c) TiO_2 NTs annealed at 500 °C and (d) TiO_2 NTs annealed at 675 °C.

samples with polished non-anodized surfaces or coated with amorphous TiO_2 NTs.

CRediT authorship contribution statement

Juliana Rios: Investigation, Writing – original draft. **Victor N. Santini:** Investigation, Validation. **Karina D. Pereira:** Investigation, Formal analysis. **Augusto D. Luchessi:** Writing – review & editing. **Éder S.N. Lopes:** Writing – review & editing. **Rubens Caram:** Writing – review & editing. **Alessandra Cremasco:** Conceptualization, Writing – original draft, Supervision, Visualization.

Declaration of Competing Interest

The authors declare that they have no known competing financial interests or personal relationships that could have appeared to influence the work reported in this paper.

Acknowledgements

The authors gratefully acknowledge the CTI and Dra. Michele Ordnicki da Silva for contact angle studies and the LNNano/CNPEM for access to the SEM facilities. The authors are thankful to the Brazilian research funding agencies, State of São Paulo Research Foundation - FAPESP (grants #2014/00159-2, #2018/18293-8, and #2019/06951-3), and National Council for Scientific and Technological Development - CNPq (grant #407412/2018-2) for their financial support.

References

[1] M. Long, H.J. Rack, Titanium alloys in total joint replacement–a materials science perspective, Biomaterials 19 (1998) 1621–1639, https://doi.org/10.1016/S0142-9612(97)00146-4.
[2] G. Yamako, D. Janssen, S. Hanada, T. Anijs, K. Ochiai, K. Totoribe, E. Chosa, N. Verdonschot, Improving stress shielding following total hip arthroplasty by using a femoral stem made of β type Ti-33.6Nb-4Sn with a Young's modulus gradation, J. Biomech. 63 (2017) 135–143, https://doi.org/10.1016/j.jbiomech.2017.08.017.
[3] E.S.N. Lopes, R.J. Contieri, S.T. Button, R. Caram, Femoral hip stem prosthesis made of graded elastic modulus metastable β Ti Alloy, Mater. Des. 69 (2015) 30–36, https://doi.org/10.1016/j.matdes.2014.11.040.
[4] D. Chiba, N. Yamada, Y. Mori, M. Oyama, S. Ohtsu, Y. Kuwahara, K. Baba, H. Tanaka, T. Aizawa, S. Hanada, E. Itoi, Mid-term results of a new femoral prosthesis using Ti-Nb-Sn alloy with low Young's modulus, BMC Musculoskelet. Disord. 22 (2021) 1–9, https://doi.org/10.1186/s12891-021-04879-1.
[5] J.M. Chaves, O. Florêncio, P.S. Silva, P.W.B. Marques, C.R.M. Afonso, Influence of phase transformations on dynamical elastic modulus and anelasticity of beta Ti–Nb–Fe alloys for biomedical applications, J. Mech. Behav. Biomed. Mater. 46 (2015) 184–196, https://doi.org/10.1016/j.jmbbm.2015.02.030.
[6] S. Ehtemam-Haghighi, Y. Liu, G. Cao, L.C. Zhang, Phase transition, microstructural evolution and mechanical properties of Ti-Nb-Fe alloys induced by Fe addition, Mater. Des. 97 (2016) 279–286, https://doi.org/10.1016/j.matdes.2016.02.094.
[7] C.N. Lopes, C. Augusto, F. Salvador, D.R. Andrade, A. Cremasco, K.N. Campo, Microstructure, mechanical properties, and electrochemical behavior of Ti-Nb-Fe alloys applied as biomaterials, Metall. Mater. Trans. A 47 (2016) 3213–3226, https://doi.org/10.1007/s11661-016-3411-0.
[8] A. Biesiekierski, J. Lin, Y. Li, D. Ping, Y. Yamabe-Mitarai, C. Wen, Investigations into Ti-(Nb,Ta)-Fe alloys for biomedical applications, Acta Biomater. 32 (2016) 336–347, https://doi.org/10.1016/j.actbio.2015.12.010.
[9] A.K. Suzuki, K.N. Campo, E.B. Fonseca, L.C. Araújo, F.C.G. Gandra, É.S.N. Lopes, Appraising the potential of Zr-based biomedical alloys to reduce magnetic resonance imaging artifacts, Sci. Rep. 10 (2020) 1–7, https://doi.org/10.1038/s41598-020-59247-1.
[10] Q. Li, P. Miao, J. Li, M. He, M. Nakai, M. Niinomi, A. Chiba, T. Nakano, X. Liu, K. Zhou, D. Pan, Effect of Nb content on microstructures and mechanical properties of Ti-xNb-2Fe alloys, J. Mater. Eng. Perform. 28 (2019) 5501–5508, https://doi.org/10.1007/s11665-019-04250-5.
[11] S. Oh, C. Daraio, L. Chen, T.R. Pisanic, R.R. Fin, S. Jin, Significantly accelerated osteoblast cell growth on aligned TiO_2 nanotubes, Biomed Mater. Res. - Part A 78 (2006) 97–103, https://doi.org/10.1002/jbm.a.
[12] K.S. Brammer, C.J. Frandsen, S. Jin, TiO_2 nanotubes for bone regeneration, Trends Biotechnol. 30 (2012) 315–322, https://doi.org/10.1016/j.tibtech.2012.02.005.
[13] S. Minagar, J. Wang, C.C. Berndt, E.P. Ivanova, C. Wen, Cell response of anodized nanotubes on titanium and titanium alloys, J. Biomed. Mater. Res. - Part A. 101A (2013) 2726–2739, https://doi.org/10.1002/jbm.a.34575.
[14] A. Roguska, M. Pisarek, A. Belcarz, L. Marcon, M. Holdynski, M. Andrzejczuk, M. Janik-Czachor, Improvement of the bio-functional properties of TiO_2 nanotubes, Appl. Surf. Sci. 388 (2016) 775–785, https://doi.org/10.1016/j.apsusc.2016.03.128.
[15] W. Yang, C. Deng, P. Liu, Y. Hu, Z. Luo, K. Cai, Sustained release of aspirin and Vitamin C from titanium nanotubes: an experimental and stimulation study, Mater. Sci. Eng. C. 64 (2016) 139–147, https://doi.org/10.1016/j.msec.2016.03.055.
[16] B. Munirathinam, L. Neelakantan, Role of crystallinity on the nanomechanical and electrochemical properties of TiO_2 nanotubes, J. Electroanal. Chem. 770 (2016) 73–83, https://doi.org/10.1016/j.jelechem.2016.03.032.
[17] W.Q. Yu, Y.L. Zhang, X.Q. Jiang, F.Q. Zhang, In vitro behavior of MC3T3-E1 preosteoblast with different annealing temperature titania nanotubes, Oral Dis. 16 (2010) 624–630, https://doi.org/10.1111/j.1601-0825.2009.01643.x.
[18] W.Q. Yu, X.Q. Jiang, F.Q. Zhang, L. Xu, The effect of anatase TiO_2 nanotube layers on MC3T3-E1 preosteoblast adhesion, proliferation, and differentiation, J. Biomed. Mater. Res. - Part A. 94 (2010) 1012–1022, https://doi.org/10.1002/jbm.a.32687.
[19] J. He, W. Zhou, X. Zhou, X. Zhong, X. Zhang, P. Wan, B. Zhu, W. Chen, The anatase phase of nanotopography titania plays an important role on osteoblast cell morphology and proliferation, J. Mater. Sci. Mater. Med. 19 (2008) 3465–3472, https://doi.org/10.1007/s10856-008-3505-3.
[20] A.Z. Fatichi, M.G. de Mello, K.D. Pereira, L.G.M. Antonio, A.D. Luchessi, R. Caram, A. Cremasco, Crystalline phase of TiO_2 nanotube arrays on Ti–35Nb–4Zr alloy: Surface roughness, electrochemical behavior and cellular response, Ceram. Int. 48 (2022) 5154–5161, https://doi.org/10.1016/j.ceramint.2021.11.054.
[21] D. Khudhair, A. Bhatti, Y. Li, H.A. Hamedani, H. Garmestani, P. Hodgson, S. Nahavandi, Anodization parameters influencing the morphology and electrical properties of TiO_2 nanotubes for living cell interfacing and investigations, Mater. Sci. Eng. C 59 (2016) 1125–1142, https://doi.org/10.1016/j.msec.2015.10.042.
[22] C. Li, Y. Ni, J. Gong, Y. Song, T. Gong, X. Zhu, A review: research progress on the formation mechanism of porous anodic oxides, Nanoscale Adv. 4 (2022) 322–333, https://doi.org/10.1039/d1na00624j.
[23] P. Li, J. Wang, L. Liu, J. Ma, Y. Ni, H. Wang, Y. Song, The effect of atmospheric pressure on the growth rate of TiO_2 nanotubes: evidence against the field-assisted dissolution theory, Electrochem. Commun. 132 (2021) 107146, https://doi.org/10.1016/j.elecom.2021.107146.
[24] J.M. Macak, H. Tsuchiya, A. Ghicov, K. Yasuda, R. Hahn, S. Bauer, P. Schmuki, TiO_2 nanotubes: self-organized electrochemical formation, properties and applications, Curr. Opin. Solid State Mater. Sci. 11 (2007) 3–18, https://doi.org/10.1016/j.cossms.2007.08.004.
[25] Z. Lockman, S. Sreekantan, S. Ismail, L. Schmidt-mende, J.L. Macmanus-driscoll, Influence of anodisation voltage on the dimension of titania nanotubes, J. Alloys Compd. 503 (2010) 359–364, https://doi.org/10.1016/j.jallcom.2009.12.093.
[26] F. Nasirpouri, I. Yousefi, E. Moslehifard, J. Khalil-Allafi, Tuning surface morphology and crystallinity of anodic TiO_2 nanotubes and their response to biomimetic bone growth for implant applications, Surf. Coatings Technol. 315 (2017) 163–171, https://doi.org/10.1016/j.surfcoat.2017.02.006.
[27] S. Poddar, A. Bit, S. Kumar, Influence of electrolytic parameters in the formation of TiO_2 nanotubes over Ti6Al4V, Mater. Today Proc. 27 (2020) 2346–2348, https://doi.org/10.1016/j.matpr.2019.09.125.
[28] C.P. Ferreira, M.C. Gonçalves, R. Caram, R. Bertazzoli, C.A. Rodrigues, Effects of substrate microstructure on the formation of oriented oxide nanotube arrays on Ti and Ti alloys, Appl. Surf. Sci. 285 (2013) 226–234, https://doi.org/10.1016/j.apsusc.2013.08.041.
[29] D.A.G. Pérez, A.M. Jorge Junior, G.H. Asato, J.C. Lepretre, V. Roche, C. Bolfarini, W.J. Botta, Surface anodization of the biphasic Ti13Nb13Zr biocompatible alloy: influence of phases on the formation of TiO_2 nanostructures, J. Alloys Compd. 796 (2019) 93–102, https://doi.org/10.1016/j.jallcom.2019.04.167.
[30] Z. Xu, Q. Li, S. Gao, J. Shang, Synthesis and characterization of niobium-doped TiO_2 nanotube arrays by anodization of Ti-20Nb alloys, J. Mater. Sci. Technol. 28 (2012) 865–870, https://doi.org/10.1016/S1005-0302(12)60144-3.
[31] N. Hu, N. Gao, Y. Chen, M.J. Starink, Achieving homogeneous anodic TiO_2 nanotube layers through grain refinement of the titanium substrate, Mater. Des. 110 (2016) 346–353, https://doi.org/10.1016/j.matdes.2016.07.144.
[32] L. Mohan, C. Anandan, N. Rajendran, Electrochemical behaviour and bioactivity of self-organized TiO_2 nanotube arrays on Ti-6Al-4V in Hanks' solution for biomedical applications, Electrochim. Acta 155 (2015) 411–420, https://doi.org/10.1016/j.electacta.2014.12.032.
[33] A.R. Rafieerad, A.R. Bushroa, E. Zalnezhad, M. Sarraf, W.J. Basirun, S. Baradaran, B. Nasiri-Tabrizi, Microstructural development and corrosion behavior of self-organized TiO_2 nanotubes coated on Ti–6Al–7Nb, Ceram. Int. 41 (2015) 10844–10855, https://doi.org/10.1016/j.ceramint.2015.05.025.
[34] L. Mohan, C. Anandan, N. Rajendran, Electrochemical behavior and effect of heat treatment on morphology, crystalline structure of self-organized TiO_2 nanotube arrays on Ti–6Al–7Nb for biomedical applications, Mater. Sci. Eng. C. 50 (2015) 394–401, https://doi.org/10.1016/j.msec.2015.02.013.
[35] S. Jang, H. Choe, Y. Ko, W.A. Brantley, Electrochemical characteristics of nanotubes formed on Ti–Nb alloys, Thin Solid Films 517 (2009) 5038–5043, https://doi.org/10.1016/j.tsf.2009.03.166.
[36] W. Kim, H. Choe, Y. Ko, W.A. Brantley, Nanotube morphology changes for Ti – Zr alloys as Zr content increases, Thin Solid Films 517 (2009) 5033–5037, https://doi.org/10.1016/j.tsf.2009.03.165.
[37] H. Tsuchiya, T. Akaki, J. Nakata, D. Terada, N. Tsuji, Y. Koizumi, Y. Minamino, P. Schmuki, S. Fujimoto, Metallurgical aspects on the formation of self-organized anodic oxide nanotube layers, Electrochim. Acta 54 (2009) 5155–5162, https://doi.org/10.1016/j.electacta.2009.02.038.
[38] D. Niu, A. Han, H. Cheng, S. Ma, M. Tian, L. Liu, Effects of organic solvents in anodization electrolytes on the morphology and tube-to-tube spacing of TiO_2

nanotubes, Chem. Phys. Lett. 735 (2019), 136776, https://doi.org/10.1016/j.cplett.2019.136776.
[39] S. Ozkan, A. Mazare, P. Schmuki, Critical parameters and factors in the formation of spaced TiO_2 nanotubes by self-organizing anodization, Electrochim. Acta. 268 (2018) 435–447, https://doi.org/10.1016/j.electacta.2018.02.120.
[40] N. Hu, Y. Wu, L. Xie, S.M. Yusuf, N. Gao, M.J. Starink, L. Tong, P.K. Chu, H. Wang, Enhanced interfacial adhesion and osseointegration of anodic TiO_2 nanotube arrays on ultra-fine-grained titanium and underlying mechanisms, Acta Biomater. 106 (2020) 360–375, https://doi.org/10.1016/j.actbio.2020.02.009.
[41] D.A.H. Hanaor, C.C. Sorrell, Review of the anatase to rutile phase transformation, J. Mater. Sci. 46 (2011) 855–874, https://doi.org/10.1007/s10853-010-5113-0.
[42] R. Hang, F. Zhao, X. Yao, B. Tang, P.K. Chu, Self-assembled anodization of NiTi alloys for biomedical applications, Appl. Surf. Sci. 517 (2020), 146118, https://doi.org/10.1016/j.apsusc.2020.146118.
[43] B. Munirathinam, L. Neelakantan, Titania nanotubes from weak organic acid electrolyte: fabrication, characterization and oxide film properties, Mater. Sci. Eng. C. 49 (2015) 567–578, https://doi.org/10.1016/j.msec.2015.01.045.
[44] M. Motola, L. Hromadko, J. Prikryl, H. Sopha, M. Krbal, J.M. Macak, Intrinsic properties of high-aspect ratio single- and double-wall anodic TiO_2 nanotube layers annealed at different temperatures, Electrochim. Acta 352 (2020), 136479, https://doi.org/10.1016/j.electacta.2020.136479.
[45] S. Fung, B. Yang, C.K. Ng, M.K. Fung, C.C. Ling, A.B. Djurĭ, Annealing study of titanium oxide nanotube arrays, Mater. Chem. Phys. 130 (2011) 1227–1231, https://doi.org/10.1016/j.matchemphys.2011.08.063.
[46] H. Li, F. Ren, Q. Li, J. Yang, Y. Wang, Z. Cheng, Spin-flip effect enhanced photocatalytic activity in Fe and single-electron-trapped oxygen vacancy co-doped TiO_2, Appl. Surf. Sci. 457 (2018) 633–643, https://doi.org/10.1016/j.apsusc.2018.06.201.
[47] S. Poddar, A. Bit, S.K. Sinha, A study on influence of anodization on the morphology of titania nanotubes over Ti6Al4V alloy in correlation to hard tissue engineering application, Mater. Chem. Phys. 254 (2020), 123457, https://doi.org/10.1016/j.matchemphys.2020.123457.
[48] D.H. Shin, T. Shokuhfar, C.K. Choi, Wettability changes of TiO_2 nanotube, Nanotechnology 22 (2011), 315704, https://doi.org/10.1088/0957-4484/22/31/315704.
[49] J.M. Chaves, A.L.A. Escada, A.D. Rodrigues, A.P.R. Alves Claro, Characterization of the structure, thermal stability and wettability of the TiO_2 nanotubes growth on the Ti-7.5Mo alloy surface, Appl. Surf. Sci. 370 (2016) 76–82, https://doi.org/10.1016/j.apsusc.2016.02.017.
[50] A. Hamlekhan, A. Butt, S. Patel, D. Royhman, C. Takoudis, C. Sukotjo, J. Yuan, G. Jursich, M.T. Mathew, W. Hendrickson, A. Virdi, T. Shokuhfar, J. Zheng, Fabrication of anti-aging TiO_2 nanotubes on biomedical Ti alloys, PLoS One. 9 (5) (2014) e96213, https://doi.org/10.1371/journal.pone.0096213.
[51] K.S. Brammer, S. Oh, C.J. Cobb, L.M. Bjursten, H. Van Der Heyde, S. Jin, Improved bone-forming functionality on diameter-controlled TiO_2 nanotube surface, Acta Biomater. 5 (2009) 3215–3223, https://doi.org/10.1016/j.actbio.2009.05.008.